scientific reports

Check for updates

OPEN

Microstructure and properties of high entropy alloy coating obtained by laser cladding

Di Lu[1], Xiangcheng Cui[1]✉ & Jinwen Zhang[2]✉

Corrosion remains a pivotal issue that significantly reduces the lifespan of metallic materials. Laser cladding technology, renowned for its exceptional effectiveness in bolstering the surface corrosion resistance of metal materials, has garnered considerable attention and interest. We propose utilizing laser cladding technology to apply a high-entropy alloy coating onto 45# steel to enhance the properties of the substrate. After undergoing an electrochemical test, the surface of coating was covered with a smooth film. The coating demonstrated exceptional corrosion resistance and adhesion qualities. By implementing this strategy, the corrosion resistance of 45# steel members can be significantly enhanced.

Keywords Laser cladding, High entropy alloy, Corrosion resistance

Metallic materials are extensively utilized as structural components across various sectors, including construction, aerospace, and automotive manufacturing[1]. When exposed to air or liquid, the metal's surface undergoes chemical or electrochemical reactions, gradually resulting in the loss of its original performance and functionality, a process known as corrosion[2,3]. Corrosion not only shortens the lifespan of metallic materials but also compromises their structural integrity, posing potential safety hazards.

The methods for enhancing the corrosion resistance of metal encompass hot-dip galvanizing, electroplating, spraying, and laser cladding, among others[4–8]. Specifically, laser cladding is an advanced technology that involves heating the surface of the workpiece using a high-energy laser beam and depositing the powder material onto this surface to form a coating[9–12]. Typically, the coating demonstrates exceptional wear and corrosion resistance, remarkable molding accuracy, and high bonding strength with the substrate.

The type of powder material utilized in the laser cladding process is crucial in determining the performance of the coating. In recent years, HEAs have attracted significant attention owing to their superior performance across various aspects, including excellent corrosion resistance and mechanical properties[13–16]. Consequently, HEAs are anticipated to serve as an ideal raw material for laser cladding applications.

To enhance the corrosion resistance of 45# steel components, we propose the application of laser cladding technology to deposit a high-entropy alloy coating onto the surface of 45# steel. In this study, we have selected CrMnFeCoNi as the raw material due to its excellent corrosion resistance and strong adhesive strength when bonded with 45# steel. Laser cladding technology has successfully prepared a well bonded corrosion resistant coating. This approach presents a practical and effective means of improving the surface corrosion resistance of 45# steel.

Methods

Material preparation

Powders of CrMnFeCoNi High-Entropy Alloys (HEAs), with a particle size ranging from 45 to 105 micrometers and gas-atomized, were employed in the laser cladding process. The chemical components of powders were listed in Table 1, the chemical components of substrate were also shown in this table. The powder had been dried first at 120 ℃ in a low vacuum oven for 1 h before were drying by vacuum oven before using. Laser cladding experiments were carried out utilizing a coaxial powder feed laser cladding system supplied with a 6 kW fiber laser. The powder particles were blown from four channels, which are designed to focus the powder particles on the substrate surface as shown in Fig. 1. The laser beam was directed and focused onto the substrate surface, creating a focal spot with a diameter of approximately 1.5 mm. These experiments were conducted within a controlled working chamber that was saturated with argon gas, ensuring that the oxygen concentration

[1]School of Materials Science and Engineering, Dalian Jiaotong University, Dalian 116028, China. [2]Guangdong Key Laboratory of Materials and Equipment in Harsh Marine Environment, Guangzhou Maritime University, Guangzhou 510725, China. ✉email: 18340807307@163.com; zjw@gzmtu.edu.cn

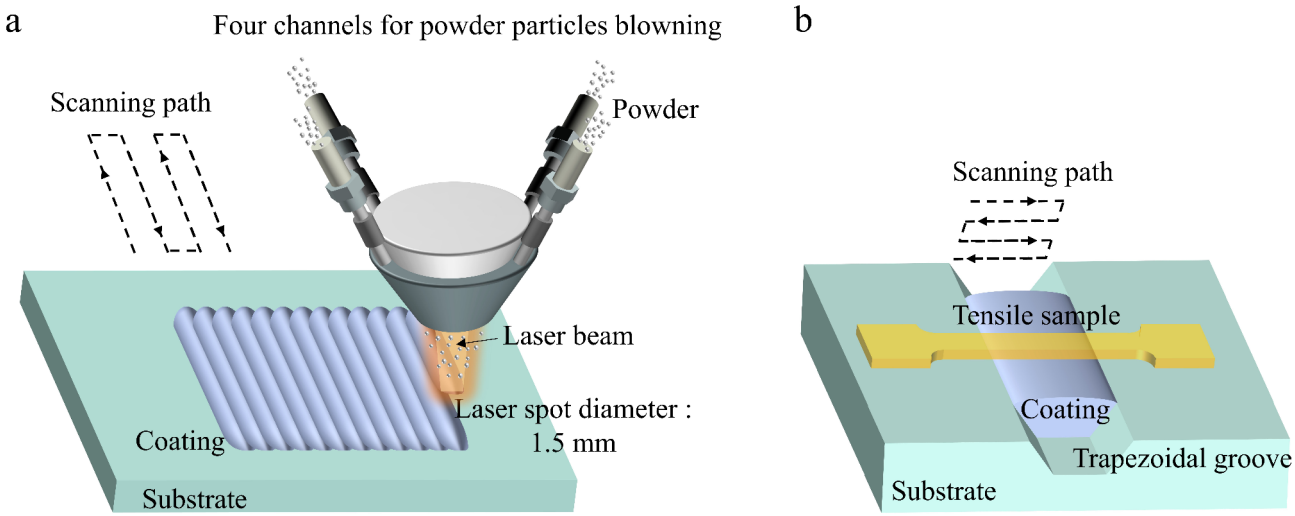

Fig. 1. Schematic diagram of laser clad on the 45# steel substrate.

Element	Fe (at%)	Cr (at%)	Mn (at%)	Co (at%)	Ni (at%)	C (at%)	*P* (at%)	Si (at%)
Substrate	97.38	0.09	1.29	-	0.17	0.47	0.14	0.46
Powder	20.21	20.35	20.28	19.89	19.26	-	-	-

Table 1. Chemical analyses of the substrate and powder.

was maintained at less than 10 ppm. Simultaneously, argon was used as a shielding gas for the laser head. Furthermore, we cladding a coating of HEAs to a trapezoidal groove to assess the bonding strength between the coating and the substrate, as illustrated on the left side of Fig. 1b.

Microstructural characterization

The laser-clad HEA coating's microstructure was examined using a Zeiss Ultra 55 field-emission scanning electron microscopes (SEM). The corrosive agent utilized in SEM was $CuSO_4 \cdot 5H_2O + H_2SO_4 + HCl + H_2O$.

Mechanical properties testing

Dog-bone-shaped tensile specimens, measuring 30 mm in length, 12 mm in width, and 2 mm in thickness at the gauge section, were obtained from the laser-clad samples through the process of electrical discharge machining. These specimens underwent tensile testing at room temperature on an MTS universal testing machine (model E43.104), with a strain rate of 1×10^{-1}. The tensile strain was determined by dividing the total elongation (measured using a standard extensometer) by the initial gauge length.

Electrochemical test

The electrochemical test was conducted using an electrochemical workstation, employing the classical three-electrode system. In this setup, the samples were utilized as the working electrode, while a platinum sheet served as the auxiliary electrode, and a reference electrode was provided by an Ag/AgCl electrode. Prior to initiating the corrosion test, the sample surfaces were polished to a 4000 grit smoothness using sandpaper. The test was performed at room temperature, with the samples submerged in a 3.5% NaCl solution. The measurements of the anodic polarization curve began at – 1.5 V and terminated at 1 V, employing a scan rate of 0.005 V/s.

Result

Microstructure

Figure 2 depicts the cross-sectional microstructure of laser cladding coatings. Figure 2a displays a low-magnification photograph of the crack-free cladding sample, revealing an absence of noticeable pores within the coating. Furthermore, there are notable distinctions between the heat affect zone and the substrate. Subsequently, we examined four regions with higher magnification for further analysis. According to Fig. 2b, it exhibits clear columnar morphology within the coating. There are a limited number of pores present within the interior, and no apparent cracks are visible. As depicted in Fig. 2c, it is evident that no microcracks are present in the vicinity of the interface between the substrate and the coating. This demonstrates that the coating and substrate adheres well together. From the heat affect zone to the matrix, the microstructure undergoes a transition from fine ferrite + granular pearlite to coarse ferrite + lamellar pearlite as shown in Fig. 2d and e. Alterations in microstructure can result in modifications to the mechanical properties of heat affect zone and the substrate.

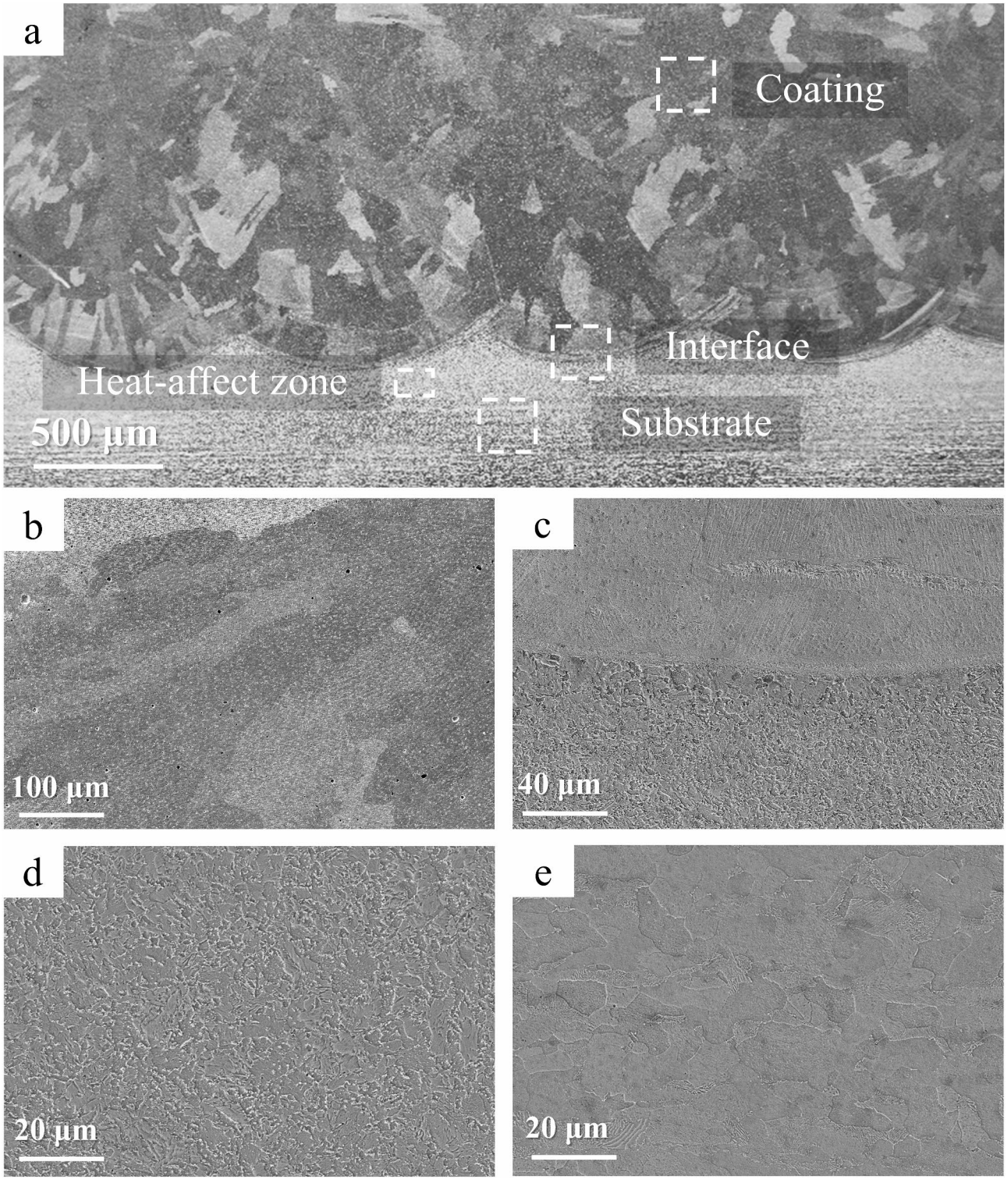

Fig. 2. Microstructure of the cross-sectional under scanning electron microscope. microstructure. (**a**) Low magnification photograph of the cladding sample. (**b**), (**c**), (**d**), (**e**) High magnification photograph of coating, interface, heat affect zone and substrate respectively.

Mechanical property

To confirm the bonding force between the coating and the substrate, a tensile test was conducted on the locally cladding sample as depicted in Fig. 3. Tensile stress is generated perpendicular to the interface during tensile process. The strain-stress curves of the locally cladding sample and substrate are shown in Fig. 3a. It can be clearly observed that compared to substrate, the yield and tensile strengths of the locally clad sample slightly

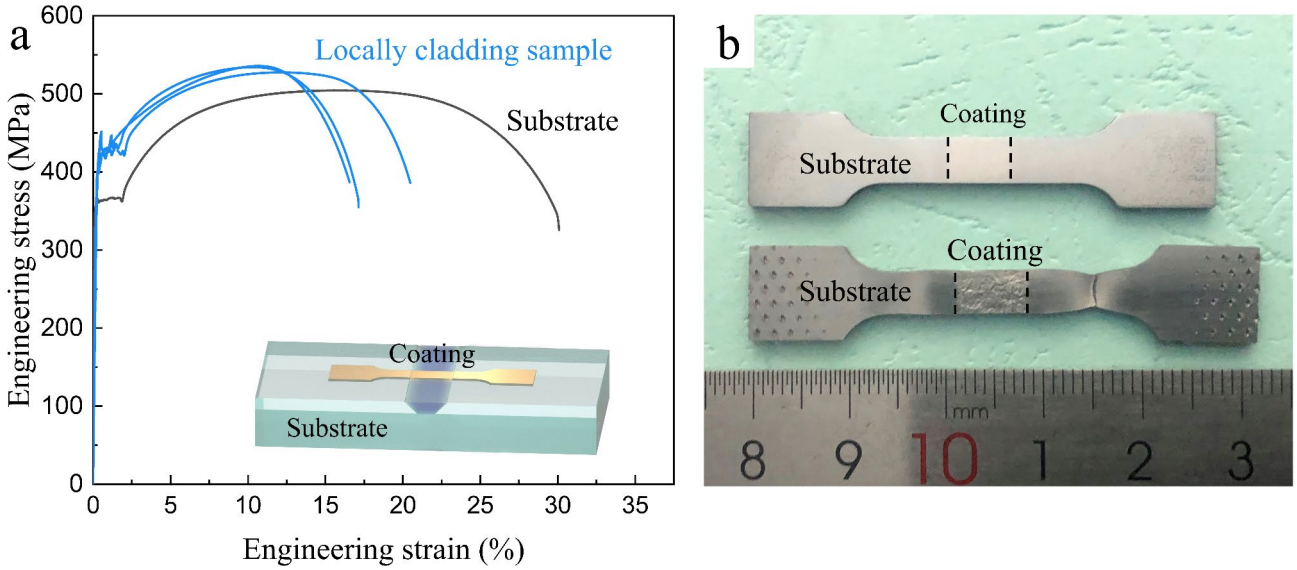

Fig. 3. Mechanical property of locally cladding sample and substrate. (**a**) Strain-stress curves of the locally cladding sample and substrate. (**b**) The fracture in the locally clad sample.

increased from 364 to 504 MPa to 431 and 535 MPa, respectively, but the elongation decreases from 16.6 to 10.6%.

A key finding is that the fracture in the locally clad sample starts in the substrate, as revealed in Fig. 3b. No failure is observed at the interface, even within the heat-affected zone. This indicates that the coating is effectively bonded to the substrate. During plastic deformation, the strain is not evenly distributed between the substrate and the cladding layer. The softer 45# steel distributes a greater strain during deformation than the harder high-entropy alloy coating, so that the overall sample appears to decrease in plasticity.

Corrosion property

The anodic polarization curves for both the coating and the substrate were obtained in a 3.5% NaCl solution. In comparison to the substrate, the HEA coating exhibits a substantial improvement in corrosion resistance when exposed to seawater solutions, evidenced by a higher corrosion potential, as illustrated in Fig. 4. The corrosion potential (Ecorr) can be derived directly from the polarization curves. Compared to substrate, the Ecorr of the cladding increased from − 1.074 to −0.775V. This significant enhancement can be ascribed to the abundant presence of Cr and Ni elements in the HEA coating, facilitating the development of a dense and highly efficacious passivation film on its surface[17].

Figure 5 presents the surface SEM image of a HEAs coating and 45# substrate after completing a polarization curve test in a 3.5% NaCl solution. Figure 5a characterizes the area near the pits in the HEAs coating. The formation of pits is attributed to the breakdown effect caused by the high potential supplied by the electrochemical workstation. Around the pits, the detachment of the passivation film can be observed, exposing the CrMnFeCoNi coating. The surface of the film is smooth and consists of numerous irregular small square-like structures, which exhibit strong corrosion resistance towards the substrate. It is clearly observable from Fig. 5b that the surface of substrate is covered with numerous tiny pits and a small amount of oxides. These oxides exhibit a porous and loose structure, making them prone to detachment, and thus, they are unable to form an effective and intact passivation film in the NaCl solution, thereby failing to provide adequate protection for the steel substrate.

Results

Here, HEAs coatings have been successfully fabricated utilizing laser cladding technology, exhibiting superior adhesion properties and corrosion resistance. The formation of smooth films during the corrosion process augments their corrosion resistance. Our work presents a highly practical and effective solution for enhancing the corrosion resistance of 45# steel.

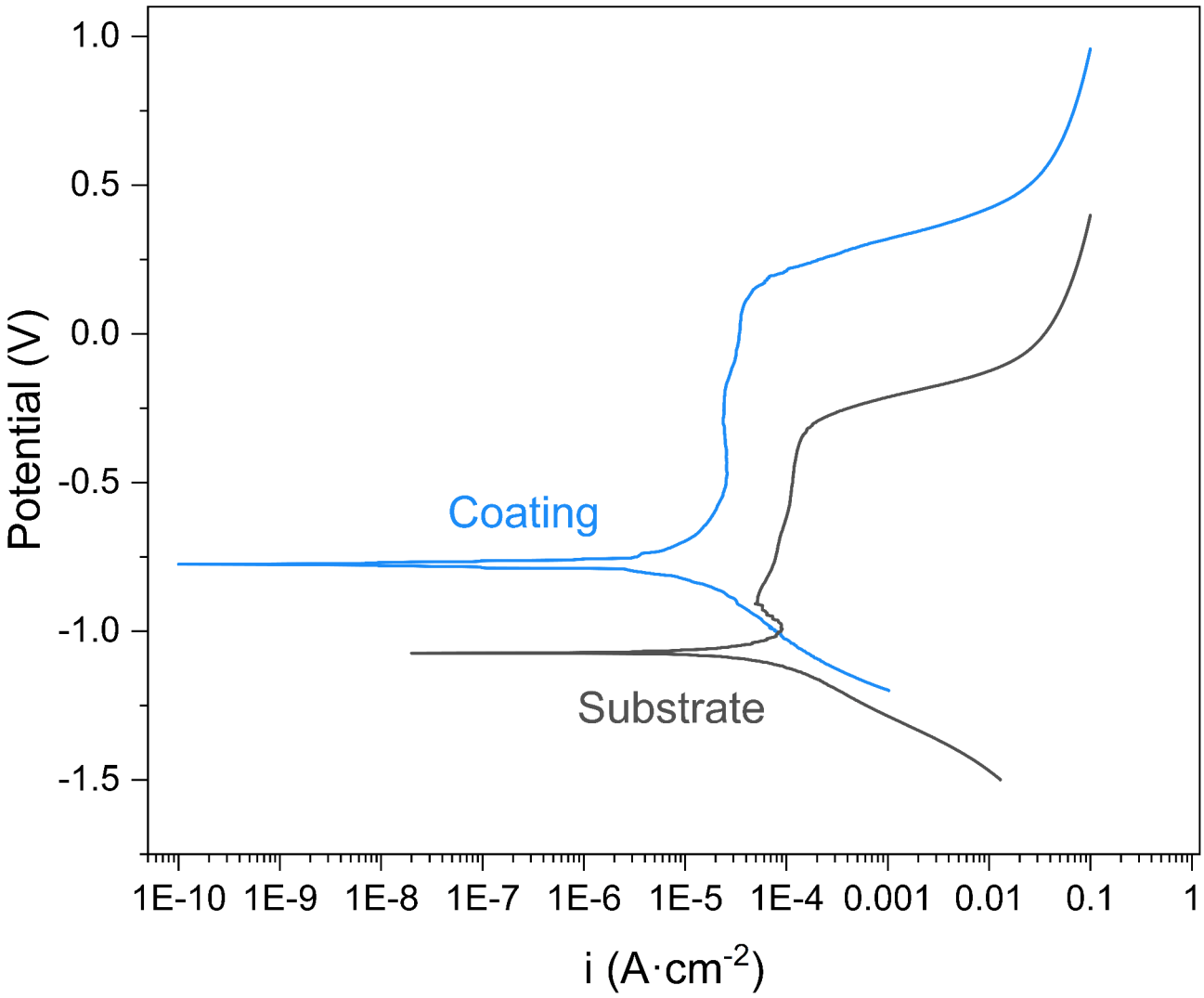

Fig. 4. Anodic polarization curve in 3.5% NaCl liquor at room temperature.

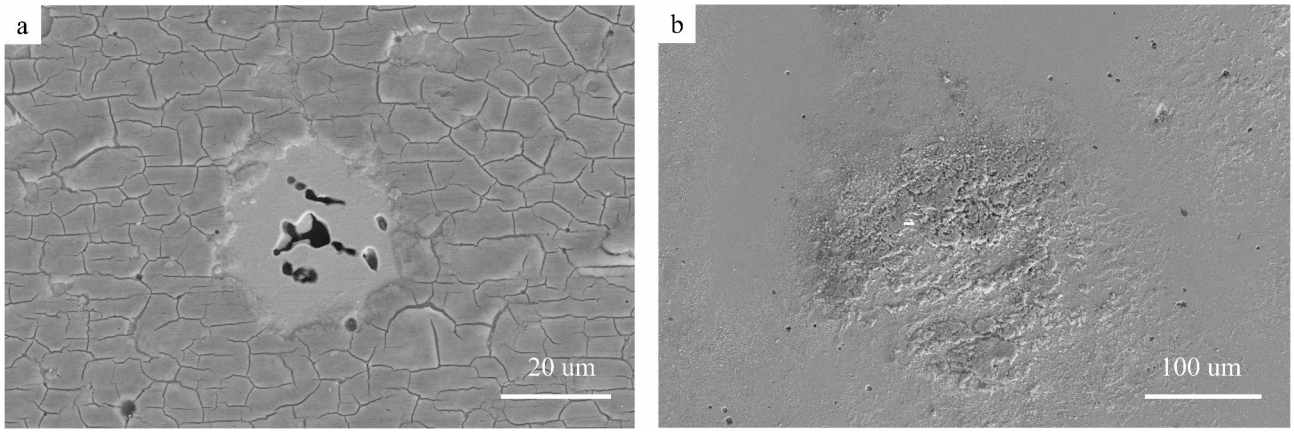

Fig. 5. The surface SEM image of coating and 45# steel after completing a polarization curve test in a 3.5% NaCl solution.

Data availability

Data is available on request from authors from Xiangcheng Cui through 18340807307@163.com.

Received: 12 January 2025; Accepted: 21 February 2025
Published online: 01 March 2025

References

1. Rohani Nejad, S., Hesari, S. & Mirbagheri, S. M. H. Effect of nickel and copper shells on mechanical properties of advanced lightweight TPU metamaterials during uniaxial compression. *Sci. Rep.* **14**, 31131 (2024).
2. Sharma, S. & Kumar, A. Recent advances in metallic corrosion Inhibition: A review. *J. Mol. Liq.* **322**, 114862 (2021).
3. Wang, L. & Chao, Y. Corrosion behavior of Fe41Co7Cr15Mo14C15B6Y2 bulk metallic glass in NaCl solution. *Mater. Lett.* **69**, 76–78 (2012).
4. Seré, P., Culcasi, J. D., Elsner, C. I. & Di Sarli A. R. Relationship between texture and corrosion resistance in hot-dip galvanized steel sheets. *Surf. Coat. Technol.* **122**, 143–149 (1999).
5. Du, L., Gao, X. Y., Wang, G. Y., Yang, C. C. & Jiang, Q. CeO2 nanoparticles decorated on porous Ni–Fe bimetallic phosphide nanosheets for high-efficient overall water splitting. *Mater. Res. Lett.* **11**, 159–167 (2023).
6. Cui, C., Wu, M., Miao, X., Zhao, Z. & Gong, Y. Microstructure and corrosion behavior of CeO2/FeCoNiCrMo high-entropy alloy coating prepared by laser cladding. *J. Alloys Compd.* **890**, 161826, (2022).
7. Suárez, G., Niculita-Hirzel, H., Correia, D., Pralong, J. A. & Vernez, D. A proposed synergetic mechanism for metal fume fever involving ZnO and Fe3O4 nanoparticles. *Sci. Rep.* **12**, 15643 (2022).
8. Bai, M. et al. Preparation and properties of polyurethane cold galvanizing coatings with phosphoric acid modified zinc powder. *Surf. Coat. Technol.* **489**, 131128 (2024).
9. Sun, S. et al. Preparing WC-Ni coatings with laser cladding technology: A review. *Mater. Today Commun.*, **106939**, (2023).
10. Zhu, Q., Liu, Y. & Zhang, C. Laser cladding of CoCrFeNi high-entropy alloy coatings: compositional homogeneity towards improved corrosion resistance. *Mater. Lett.* **318**, 132133 (2022).
11. Fu, A. et al. Controlling of cellular substructure and its effect on mechanical properties of FeCoCrNiMo0. 2 high entropy alloy fabricated by selective laser melting. *Mater. Sci. Engineering: A*. **901**, 146547 (2024).
12. Fu, J. et al. Microstructure and mechanical properties of WC-12Co cemented carbide fabricated by laser powder bed fusion on a WC-20Co cemented carbide substrate. *J. Mater. Res. Technol.*, (2024).
13. Elbakhshwan, M. et al. Corrosion and thermal stability of CrMnFeNi high entropy alloy in molten FLiBe salt. *Sci. Rep.* **9**, 18993 (2019).
14. Reddy, S. et al. Nanostructuring with structural-compositional dual heterogeneities enhances strength-ductility synergy in eutectic high entropy alloy. *Sci. Rep.* **9**, 11505 (2019).
15. Yang, M., Xu, J., Huang, J., Zhang, L. & Luo, J. Wear resistance of N-doped CoCrFeNiMn high entropy alloy coating on the Ti-6Al-4V alloy. *J. Therm. Spray Technol.*, 1–11, (2024).
16. Xu, X. et al. Cryo-rolling and annealing-mediated phase transformation in Al5Ti2. 5Fe25Cr25Ni42. 5 high-entropy alloy: experimental, phase-field and CALPHAD investigation. *J. Mater. Sci. Technol.* **219**, 307–325 (2025).
17. Guo, P. et al. Unveiling the transpassive film failure of 3D printing transition alloys. *Corros. Sci.* **204**, 110412 (2022).

Acknowledgements

This work is supported by the Guangdong Province Special Funding Project for the Development of Marine Economy under Grant No. GDNRC [2024]41.

Author contributions

Di Lu: Writing – original draft, Conceptualization, Software, Methodology, Data curation.Xiangcheng Cui: Writing – review & editing, Supervision, Project administration, Funding acquisition, Investigation, Resources. Jinwen Zhang: Data curation, Funding acquisition.

Declarations

Competing interests

The authors declare no competing interests.

Additional information

Correspondence and requests for materials should be addressed to X.C. or J.Z.

Reprints and permissions information is available at www.nature.com/reprints.

Publisher's note Springer Nature remains neutral with regard to jurisdictional claims in published maps and institutional affiliations.